Review

Evolution of Auriferous Fluids in the Kraaipan-Amalia Greenstone belts: Evidence from Mineralogical and Isotopic Constraints

Kofi Adomako-Ansah , Napoleon Quaye Hammond * , Yuichi Morishita , Daizo Ishiyama

Posted Date: 28 August 2024

doi: 10.20944/preprints202408.2025.v1

Keywords: Kraaipan; Amalia; greenstone belt; gold; oxide BIF; strontium isotopes; South Africa; Kaapvaal Craton

 doi:10.20944/preprints202408.2025.v1

Review

Evolution of Auriferous Fluids in the Kraaipan-Amalia Greenstone belts: Evidence from Mineralogical and Isotopic Constraints

Kofi Adomako-Ansah [1], Napoleon Q. Hammond [2] and Yuichi Morishita [3],and Daizo Ishiyama [4]

[1] Department of Geological Engineering, University of Mines and Technology, P.O. Box 237, Tarkwa, Ghana
[2] Department of Geology and Mining, School of Physical and Mineral Sciences, University of Limpopo, Private Bag X1106, Sovenga 0727, South Africa
[3] Faculty of Science, Centre for Integrated Research and Education of Natural Hazards, Shizuoka University, 836 Ohya, Suruga-ku, Shizuoka, 422-8529, Japan
[4] Graduate School of International Resource Sciences, Akita University, 1-1 Tegata-gakuen machi, Akita 010-8502, Japan
* Correspondence: napoleon.hammond@ul.ac.za

Abstract: The Kraaipan and Amalia greenstone belts in South Africa occurs in the western part of the Kaapvaal Craton. The two belts stretch discontinuously in an approximately north-south orientation over a distance of about 250 km from southern Botswana in the north to the Vaal River near Christiana in the south and are separated by a distance of about 90 km. Gold mineralization is hosted in banded iron-formation at both the Kalahari Goldridge deposit (Kalgold) in the Kraaipan greenstone belt in the north, and the Amalia deposit in the Amalia greenstone belt in the south, with the mineralization associated with quartz-carbonate veins. The footwall of these deposits is generally composed of mafic volcanic schist and hanging wall consisting of graywackes, schist and shale units.The Kalgold and Amalia gold deposits show some variation in the redox condition of the mineralizing system, mineralization temperatures and fluid chemistry. The ore mineral assemblage is characterized by magnetite-pyrrhotite-pyrite at Kalgold, which is indicative of reducing conditions, and magnetite-hematite-pyrite assemblage at Amalia that suggest a relatively oxidizing environment. Average mineralizing temperatures determined from chlorite geothermometry were relatively higher at the Kalahari Goldridge deposit ranging from 350 to 400^{o}C compared to 335 to 370^{o}C (mean, 352± 18, n = 113) at Amalia. The composition of the fluids derived from fluid inclusions are indicative of low salinity H_2O-CH_4-CO_2-rich fluids at Kalgold against relatively H_2O-CO_2-rich fluids at Amalia.Evidence from strontium-carbon-oxygen isotopic ratios from carbonates suggests differences in redox conditions in the deposits could be attributed to different flow pathways by the evolving fluid from a common source (with minimum $^{87}Sr/^{86}Sr$=0.70354) to the sites of gold deposition; with significant ore fluid interaction with thick sequence of carbonaceous meta-pelitic rock units at the Kalahari Goldridge deposit, that is absent in the Amalia deposit.

Keywords: Kraaipan; Amalia; greenstone belt; gold; oxide BIF; strontium isotopes; South Africa; Kaapvaal Craton

1. Introduction

Several studies on Archaean orogenic gold deposits (e.g., Kerrick 1989; Ho et al., 1992; Groves *et al.* 1998; Goldfarb and Groves, 2015; Groves *et al.*, 2020) are documented to have been formed from ore-forming fluids that originated from deep within the crust, along crustal scale faults or fissures through which these fluids have migrated to depositional sites of ore metals and associated minerals. The stable isotope data associated with most of these studies have been unable to clearly define the origin of ore-forming fluids associated with such deposits due to overlap of isotopic signatures among fluid sources. The application of radiogenic isotopes, particularly strontium (Sr) in recent years, have proven to be a useful tool in understanding the source reservoir and flow pathways of these fluids (e.g., Glodny and Grauert, 2009; Toki et al. 2022; Kim et al., 2004). The flow pathways

 doi:10.20944/preprints202408.2025.v1

can provide significant insight to the nature of water-rock interaction between the fluid and the rocks encountered during fluid migration; thus, providing important information on the nature and evolution of the hydrothermal fluid in ore deposit systems. The Kraaipan and Amalia greenstone belts in South Africa is a N-S trending, laterally discontinuous structure that are spatially associated with granitoids of similar petrological characteristics and age (Figure 1). The basement rocks of these greenstone belts are Archaean TTG gneisses (Anhaeusser and Walraven 1999). Epigenetic banded iron-formation (BIF)-hosted gold deposits within the Kraaipan-Amalia terrane include the Kalahari Goldridge deposit in the Kraaipan greenstone belt (to the north) and the Amalia deposit in the Amalia greenstone belt (to the south) (Figure 1), and are separated about 90 km from each other. The hanging wall units in both deposits comprises metasedimentary rocks of shales and schists, and footwall comprises mafic volcanic schists (Figures 2 and 3). However, local lithological variations occur between the BIF and footwall at the Kalahari Goldridge deposit (Hammond and Moore 2006).

Figure 2

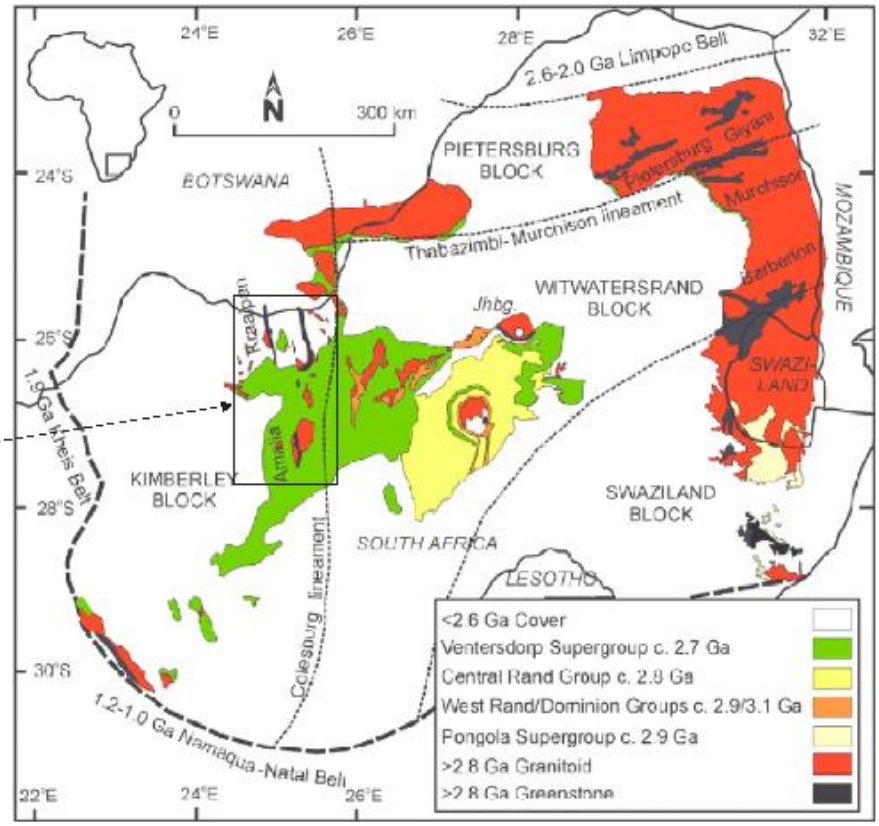

Figure 1: Geological map of the Kaapvaal Craton showing the location of the Kraaipan and Amalia greenstone belt in the Kimberley Block. Modified after Frimmel (2014).

 doi:10.20944/preprints202408.2025.v1

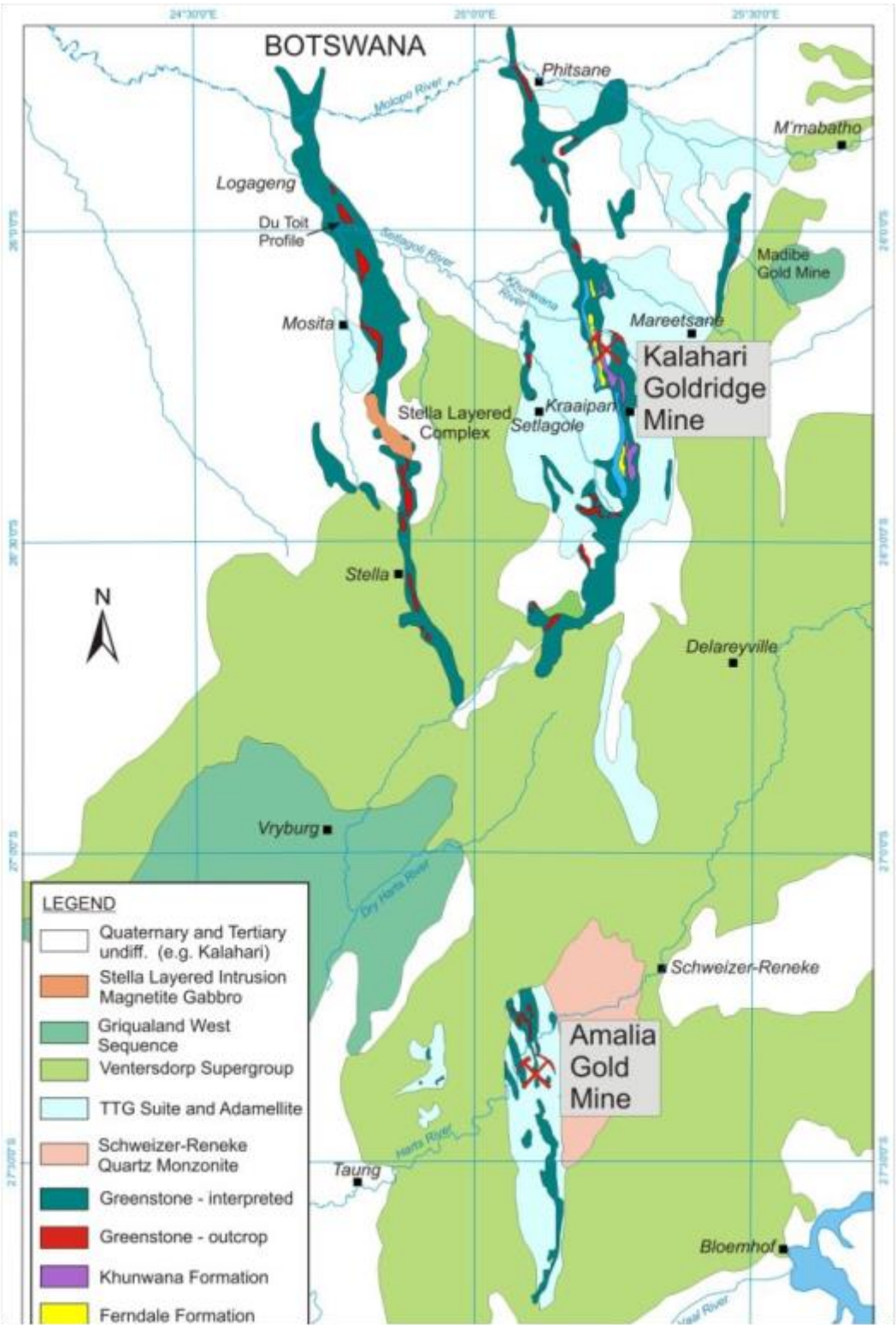

Figure 2: Regional geological map of the Kraaipan and Amalia greenstone belts with the location of the Kalahari Goldridge and Amalia gold deposits.

 doi:10.20944/preprints202408.2025.v1

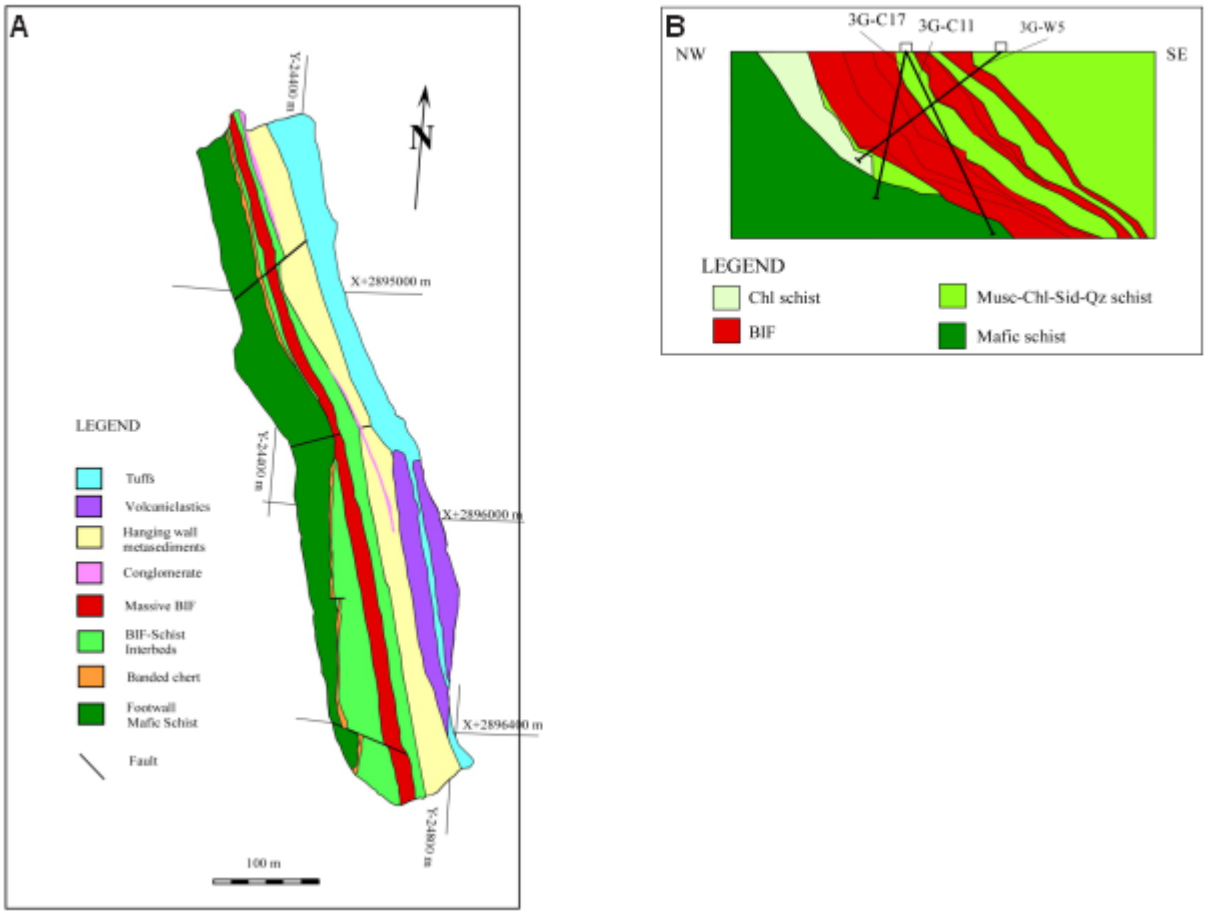

Figure 3: Local geological map of the Kalahari Goldridge, D Zone orebody (A) and the Amalia gold deposit (B).

Despite similar geological settings, the ambient conditions associated with the mineralization in these deposits exhibit some geochemical variations (Hammond *et al.* 2007, Adomako-Ansah *et al.* 2017). It is therefore not clear if the mineralizing events in these deposits were spatially linked to a unique fluid source that were modified along different flow pathways to the depositional' sites or they were discrete mineralizing events with distinct sources. A combination of Sr-C-O isotopic ratios from previous studies on the Kalahari Goldridge (Hammond *et al.* 2007, Hammond and Morishita 2009), C-O isotope on Amalia (Adomako-Ansah *et al.* 2017) and new Sr isotope data for the Amalia deposit, this paper attempts to unravel and evaluate the nature and evolution of the fluids associated with gold mineralization in the Kraaipan-Amalia terrane.

2. Geological Setting

The evolution history of the Kaapvaal craton includes the amalgamation of the ~3.7-Ga-old Witwatersrand block (to the east) and 3.2-Ga-old Kimberly block (to the west) along the Colesberg Lineament (CL) suture (Figure 1) by subduction-accretion and continent-continent collision processes that occurred at about 3.0-2.9 Ga ago (Corner *et al.* 1990, de Wit *et al.* 1992, McCourt 1995, Richardson *et al.* 2001, Schmitz *et al.* 2004, Errickson *et al.* 2009). The Kraaipan-Amalia greenstone belts are located in the Kimberly block of the Kaapvaal craton and aligned parallel to the CL. The thermo-tectonic processes is believed to have resulted in the formation of highly deformed, north-south-trending subvertical volcano-sedimentary rock units in the Kraaipan-Amalia greenstone belts that are generally fault-bounded and partially engulfed by abundant intrusive syn- to post-deformational granitoids (de Wit *et al.* 1992, Schmitz *et al.* 2004). The Kraaipan-Amalia greenstone belt is flanked to west by 3.08-2.93 Ga-old reworked TTGs and, to the east by 2.93-2.85 Ga-old Kraaipan group of post-collisional and intrusive granodioritic and magnetite-bearing quartz monzonitic plutons (Figure 1; Anhaeusser and Walraven 1999, Poujol *et al.* 2002, Robb and Meyer 1995). Spatial association

 doi:10.20944/preprints202408.2025.v1

between the Kraaipan-Amalia greenstone belts and the granodioritic-monzonitic rocks aroused speculations on a genetic link between the gold deposits within the greenstone belts and felsic igneous activity (e.g., Anhaeusser and Walraven 1999, Poujol *et al.* 2002, Robb and Meyer 1995). The greenstone belts are poorly exposed due to limited outcrop in the region. Sparse low-ridged BIF have been reported to be associated with a suite of agglomerates and accretionary lapilli tuffs (Jones and Anhaeusser 1993, Anhaeusser and Walraven 1999). Geophysical investigation conducted across the CL by de Wit and Tinker (2004) revealed that the Kraaipan-Amalia greenstone belt terrane was obducted unto the Kaapvaal craton from the east as an allochthonous unit by accretionary tectonics (de Wit and Tinker 2004).

3. Hydrothermal Alteration and Gold Mineralization

The geological, mineralogical and geochemical characteristics are detailed in Hammond and Moore (2006), Hammond *et al.* (2007), Hammond and Morishita (2009), Kiefer (2004), Adomako-Ansah *et al.* (2013) and Adomako-Ansah *et al.* (2017) and are summarized in Table 1. The host rocks to mineralization in the Kalahari Goldridge and Amalia gold deposits are magnetite-rich oxide facies BIFs (Figure 3); Hammond and Moore 2006, Adomako-Ansah *et al.* 2013). Gold mineralization in both deposits is associated with quartz-carbonate veins that cut across the oxide-facies BIF layers (Figure 4). Field observation and textural evidence in both deposits indicate carbonate alteration of the BIF was pervasive and occurred alongside sulphidized alteration haloes that surrounded the contacts and selvages between the quartz-carbonate veins and the host BIF units. Hematization of magnetite was observed at Amalia, however, it was absent at Kalahari Goldridge. Geochemical evidence showed that gold mineralization in both deposits is closely associated with the altered host rocks; typically, the carbonate-altered and highly sulphidized BIF. Replacement of magnetite by pyrite and pyrrhotite is prominent at Kalahari Goldridge (Figure 5A-C), however, there is extensive replacement of magnetite by hematite and pyrite at the Amalia deposit with minor chalcopyrite and arsenopyrite (Figure 5D-F). These observations are clearly consistent with contrasting ambient redox conditions in the ore-forming fluids during mineralization in these deposits: a reduced fluid system at Kalahari Goldridge deposit and more oxidized conditions at Amalia.

Table 1. A. Sr isotopes data of carbonates from the Amalia gold deposit, Amalia Greenstone Belt, South Africa. B. Sr isotopes data of carbonates from the Kalahari goldridge deposit, Kraaipan Greenstone Belt (From Hammond and Morishita, 2007).

A										
Sample name	**$\delta^{18}O_{SMOW}$ (per mil)**	**$\delta^{13}C_{PDB}$ (per mil)**	**$^{87}Rb/^{86}Sr$**	**Rb (ppm)**	**Sr (ppm)**	**Rb/Sr**	**1/Sr (ppm^{-1})**	**$^{87}Sr/^{86}Sr$**	**std**	**$^{87}Rb/^{86}Sr$**
C17-20	17.2	-4.0	0.010	0.55	157.20	0.004	0.006	0.703023	(±7; 2σ)	0.010
C11-5A-3	16.3	-4.5	0.076	1.00	38.15	0.026	0.026	0.703747	(±6; 2σ)	0.076
C17-15B	13.5	-5.6	1.23	1.46	3.43	0.426	0.292	0.706643	(±6; 2σ)	1.23
C17-23	16.3	-3.9	0.371	0.89	6.94	0.128	0.144	0.704895	(±6; 2σ)	0.371
N23-7A	17.4	-3.5	0.382	1.88	14.22	0.132	0.070	0.705781	(±12; 2σ)	0.382
C17-6	16.3	-4.6	0.078	2.11	78.45	0.027	0.013	0.704318	(±7; 2σ)	0.078
B										
ARC 236/11A	11.3	-5.6	0.034	0.1	23.3	0.004	0.043	0.71042	(±1; 2σ)	0.034
ARC 236/11X	10.1	-5.8	0.188	0.3	4.5	0.067	0.222	0.72325	(±1; 2σ)	0.188
ARC 236/16	15.1	-5.4	0.04	0.04	3.5	0.011	0.286	0.71138	(±1; 2σ)	0.04
MSH/W-3	9.8	-7.6	0.005	0.3	168	0.002	0.006	0.70354	(±1; 2σ)	0.005
GDP 531/9C	11.5	-6.9	0.513	0.2	1.1	0.182	0.909	0.72907	(±2; 2σ)	0.513
DZ 40/1	10.3	-6.7	0.389	0.4	2.9	0.138	0.345	0.73914	(±2; 2σ)	0.389
DZ 40/2	10.6	-6.7	0.047	0.2	12.1	0.017	0.083	0.71583	(±1; 2σ)	0.047
DZ 40/3	10.8	-6.6	0.047	0.3	18.2	0.016	0.055	0.71235	(±1; 2σ)	0.047
GDP 531/16B	10.8	-6.1	0.006	0.1	18.1	0.006	0.055	0.70564	(±2; 2σ)	0.006

std = standard deviation
Ank = ankerite
Sid = siderite

 doi:10.20944/preprints202408.2025.v1

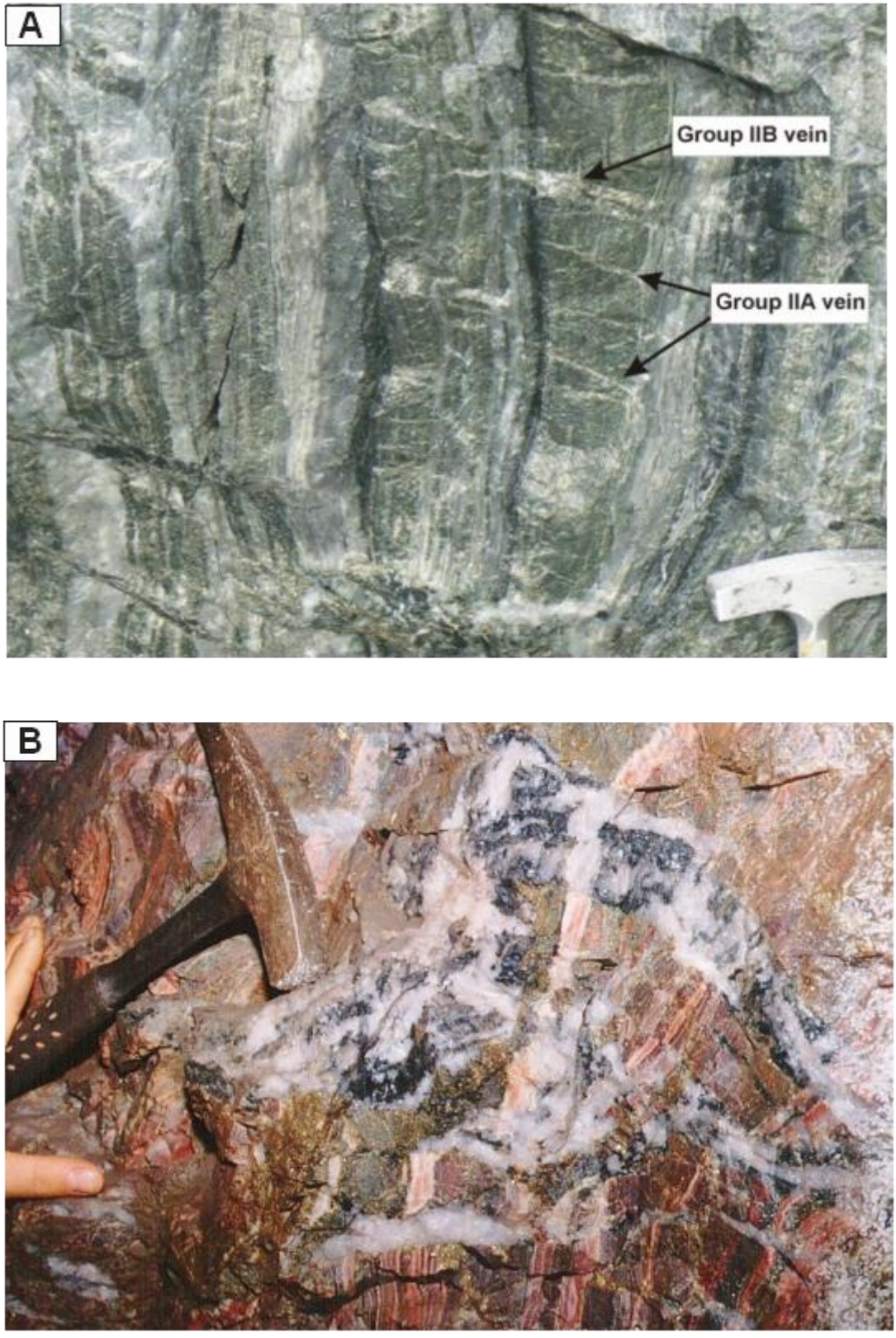

Figure 4. Photos of quartz-carbonate veins in BIF at the Kalahari Goldridge deposit (**A**) and Amalia gold deposit (**B**).

 doi:10.20944/preprints202408.2025.v1

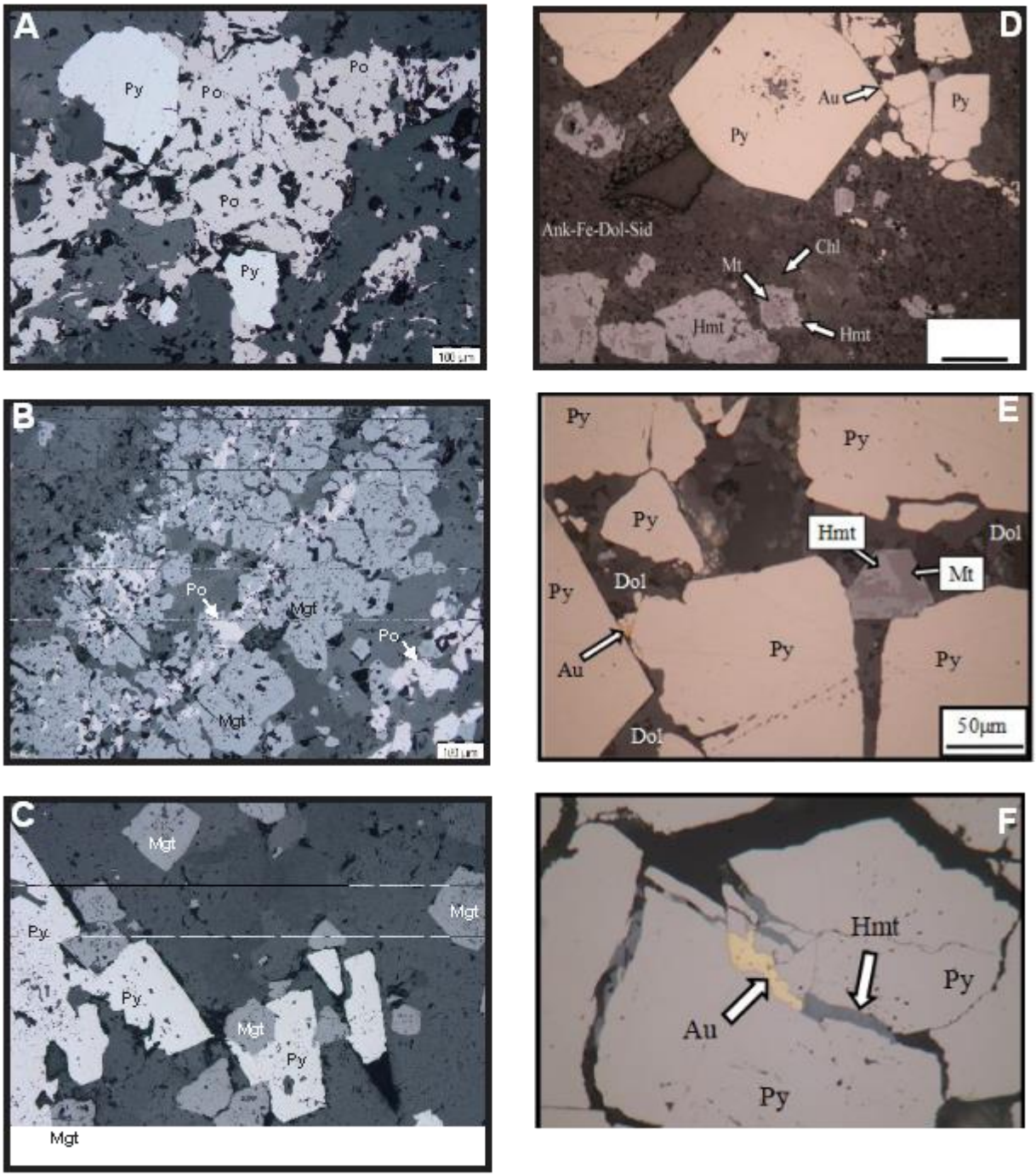

Figure 5: Textural relationships between ore minerals in BIF at the Kalahari Goldridge (A, B and C) and Amalia gold deposits (D, E and F). Po = pyrrhotite, Py = pyrite, Mgt = magnetite, Hmt = hematit e Au = gold.

The varied redox state of these deposits is further evidenced from microthermometric and Raman analyses of fluid inclusions in quartz veins that indicated low salinity NaCl-H_2O-CO_2±CH_4 compositions at the Kalahari Goldridge (Hammond *et al.* 2007) and NaCl-H_2O-CO_2 at Amalia Adomako-Ansah *et al.* 2017), Figure 6. Thus, a relatively 'pure' CO_2-rich composition characterizes the ore-forming fluid at Amalia compared to the Kalahari Goldridge, which contains significant in CH_4 in some inclusion.

 doi:10.20944/preprints202408.2025.v1

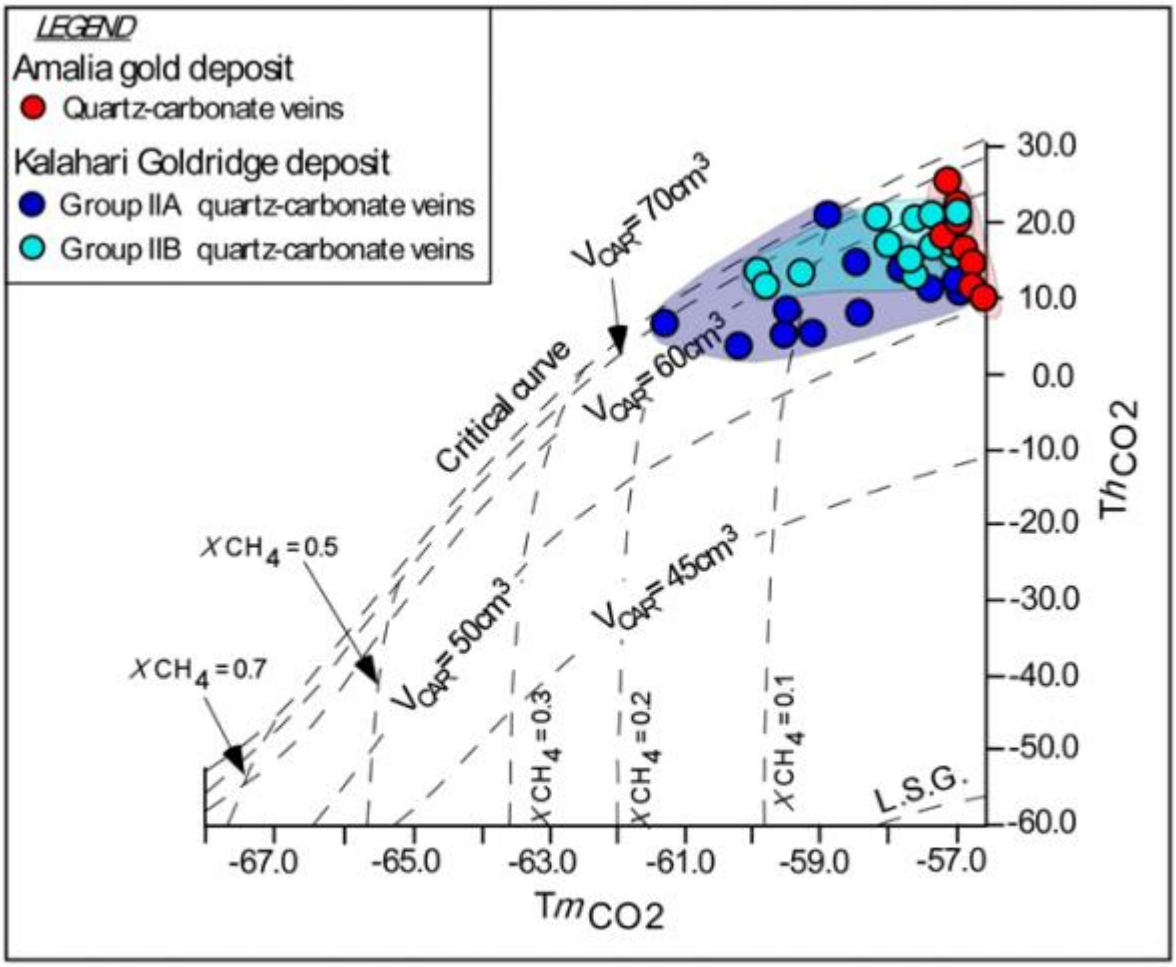

Figure 6. $TmCO_2$ versus $ThCO_2$ of fluid inclusions in quartz veins from the Kalahari Goldridge and Amalia gold deposits. The inclusions shows relatively pure CO_2-rich inclusions at Amalia compared to the Kalahari Goldridge, which have mixed CO_2-CH_4-rich inclusions.

4. Mineralization Temperatures Based on Chlorite Geothermometry

Chlorite is a common mineral which occurs in a wide range of geological environments such as diagenesis, low- to medium-grade metamorphism and hydrothermal alteration. The mineral displays a wide range of non-stoichiometric compositional variations depending on bulk composition of host rocks, particularly the Fe/(Fe+Mg) ratio, prevailing physico-chemical conditions such as temperatures, pressures, redox state during formation (Bryndzia and Scott, 1987; De Caritat et al., 1993; Vidal et al., 2016), and fluid chemistry in systems associated with hydrothermal deposits. The variation of chemical composition in chlorite has served as a useful tool to obtain information on the physico-chemical conditions during the evolution of mineralizing hydrothermal fluids. In particular, the chlorite geothermometry have been applied widely in the estimation of formation temperatures of chlorites in hydrothermally altered rocks in many ore deposits given its ubiquitous occurrence in such geological settings.

The mineralization temperatures for the Amalia and Kalahari Goldridge deposits were determined using the chlorite geothermometry data of Cathelineau and Nieva (1985) and Cathelineau (1988). The compositions of the chlorite were analysed from chlorites in mineralizing veins and hydrothermally altered BIFs. Figure 7 illustrates these ranges from 350° to 400°C at the Kalahari Goldridge deposit (Hammond et al. 2007, Hammond and Morishita, 2009), and 330° to 390°C at Amalia (Adomako-Ansah et al., 2013). However, there is an overall decrease in temperature with

 doi:10.20944/preprints202408.2025.v1

corresponding decreasing Fe/(Fe+Mg) ratio, with highest temperatures recorded in chlorites in altered BIF at Kalahari Goldridge and lowest temperatures associated with chlorites in late factures in Amalia BIF.

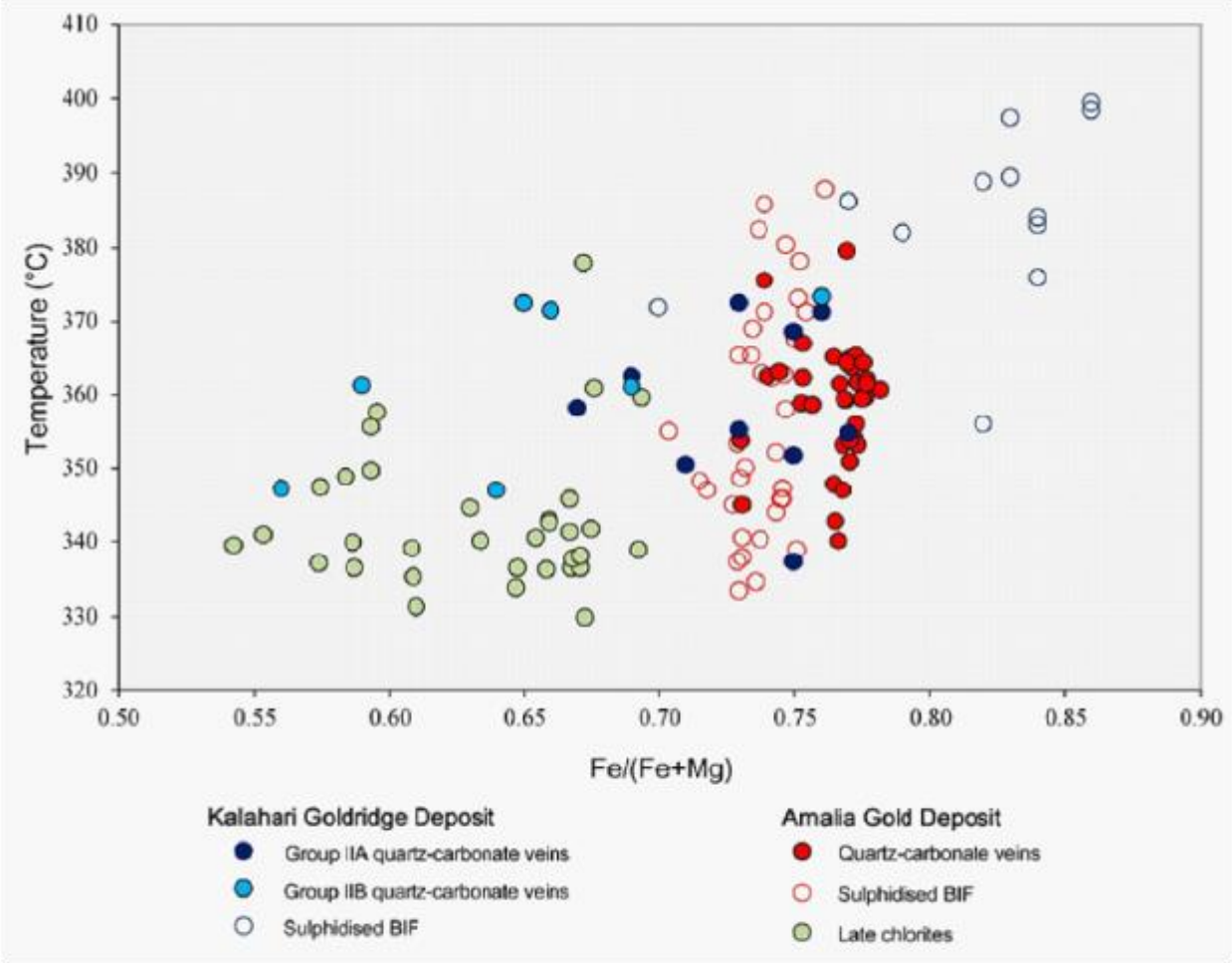

Figure 7: Temperature distribution based on chlorite geothermometry in quartz-carbonate veins and altered BIF at the Kalahari Goldridge and Amalia gold deposits showing a relatively increasing temperature variation from Amalia to the Kalahari Goldridge deposit.

5. Isotopic (Sr, C and O) Signatures and Rb Concentrations

Rubidium-strontium, carbon and oxygen isotopic systematics in carbonates from the alteration carbonates at the Amalia and Kalahari Goldridge deposits were undertaken to deduce the nature and evolution of fluids in these deposits in an attempt to define the fluid origin in the Kraaipan-Amalia terrane. The Rb-Sr isotopic technique was based on the premise that in minerals that contain relatively low concentration of Rb (<1ppm) but high concentrations of Sr such as in carbonates arising from Sr-Ca substitution due to similar ionic radii of the two elements. Hence, the $^{87}Sr/^{86}Sr$ ratio can remain relatively unchanged with time due to limited or no influence of radiogenic Sr from in-situ radioactive decay of Rb. The $^{87}Sr/^{86}Sr$ ratios may therefore, represent the approximate initial compositions of the fluids at the time of carbonate crystallization. On the basis of this premise, diagnostic fluid-rock interaction trends between evolving fluid systems and crustal components can be constructed to deduce this assertion. The Rb-Sr isotope data for Kalahari Goldridge deposit reported earlier by Hammond and Morishita (2009) and compared with new strontium isotopic signatures ($^{87}Sr/^{86}Sr$ isotopic ratios) for the Amalia gold deposit. Mineralizing quartz-carbonate veins from both deposits were crushed in a steel mortar and carbonates separated manually under

 doi:10.20944/preprints202408.2025.v1

binocular microscopes. The carbonates were subject to standard ion exchange technique and $^{87}Sr/^{86}Sr$ isotopic measurements, and trace elements concentration including Sr and Rb were determined using multicollector ICP-MS, at the Department of Earth Science and Technology, Akita University in Japan for the Amalia deposits, and the Research School of Earth Science, Australian National University for the Kalahari Goldridge deposits. Six (6) $^{87}Sr/^{86}Sr$ isotopic ratios of carbonates were determined from the Amalia veins and nine (9) $^{87}Sr/^{86}Sr$ isotopic ratios of carbonates determined for the Kalahari Goldridge deposit (Table 2). Analyses of the carbonate separates by MC-ICP-MS measurements following chemical separation of Rb and Sr by ion exchange chromatography yielded very radiogenic $^{87}Sr/^{86}Sr$ ratios range from 0.703023 to 0.706643 for the carbonates from Amalia. The Sr and Rb concentrations vary from 3.4 to 157.2 ppm and 0.6 to 2.1 ppm, respectively. The $^{87}Sr/^{86}Sr$ ratios of the vein carbonate in the Kalahari Goldridge is from 0.70354 to 0.73914, while the Sr and Rb concentrations vary from 1.1.2 to 168 ppm and 0.04 to 0.4 ppm, respectively.

Table 2. A. Sr isotopes data of carbonates from the Amalia gold deposit, Amalia Greenstone Belt, South Africa. B. Sr isotopes data of carbonates from theKalahari Goldridge, Kraaipan Greenstone Belt, South Africa (Hammond & Morishita, 2009).

Sample name	Sampled material	Host rock	Mineral	$\delta^{18}O_{SMOW}$ (per mil)	$\delta^{13}C_{PDB}$ (per mil)	$^{87}Rb/^{86}Sr$	Rb (ppm)	Sr (ppm)	Rb/Sr	1/Sr (ppm^{-1})	$^{87}Sr/^{86}Sr$		$^{87}Rb/^{86}Sr$
A													
C17-20	quartz-carbonate vein	Mineralised BIF	Ankerite	17.2	-4.0	0.010	0.55	157.20	0.004	0.006	0.703023	(±7; 2σ)	0.010
C11-5A-3	quartz-carbonate vein	Mineralised BIF	Ankerite	16.3	-4.5	0.076	1.00	38.15	0.026	0.026	0.703747	(±6; 2σ)	0.076
C17-15B	quartz-carbonate vein	Mineralised BIF	Ankerite	13.5	-5.6	1.23	1.46	3.43	0.426	0.292	0.706643	(±6; 2σ)	1.23
C17-23	quartz-carbonate vein	Mineralised BIF	Ankerite	16.3	-3.9	0.371	0.89	6.94	0.128	0.144	0.704895	(±6; 2σ)	0.371
N23-7A	quartz-carbonate vein	Mineralised BIF	Ankerite	17.4	-3.5	0.382	1.88	14.22	0.132	0.070	0.705781	(±12; 2σ)	0.382
C17-6	quartz-carbonate vein	H/W schist	Ankerite	16.3	-4.6	0.078	2.11	78.45	0.027	0.013	0.704318	(±7; 2σ)	0.078
B													
ARC 236/11A	quartz-carbonate vein IIB	Mineralised BIF	Ankerite	11.3	-5.6	0.034	0.1	23.3	0.004	0.043	0.71042	(±1; 2σ)	0.034
ARC 236/11X	quartz-carbonate vein IIB	Mineralised BIF	Siderite	10.1	-5.8	0.188	0.3	4.5	0.067	0.222	0.72325	(±1; 2σ)	0.188
ARC 236/16	quartz-carbonate vein IIA	Mineralised BIF	Siderite	15.1	-5.4	0.04	0.04	3.5	0.011	0.286	0.71138	(±1; 2σ)	0.04
MSH/W-3	quartz-carbonate vein IIA	Mineralised BIF	Ankerite	9.8	-7.6	0.005	0.3	168	0.002	0.006	0.70354	(±1; 2σ)	0.005
GDP 531/9C	quartz-carbonate vein IIA	Mineralised BIF	Siderite	11.5	-6.9	0.513	0.2	1.1	0.182	0.909	0.72907	(±2; 2σ)	0.513
DZ 40/1	quartz-carbonat	Mineralised BIF	Siderite	10.3	-6.7	0.389	0.4	2.9	0.138	0.345	0.73914	(±2; 2σ)	0.389

 doi:10.20944/preprints202408.2025.v1

DZ 40/2	e vein IIB quartz-carbonate vein IIB	Mineralised BIF	Siderite	10.6	-6.7	0.047	0.2	12.1	0.017	0.083	0.71583	(±1; 2σ)	0.047
DZ 40/3	quartz-carbonate vein IIB	Mineralised BIF	Siderite	10.8	-6.6	0.047	0.3	18.2	0.016	0.055	0.71235 (±1; 2σ)		0.047
GDP 531/16B	quartz-carbonate vein IIB	Mineralised BIF	Siderite	10.8	-6.1	0.006	0.1	18.1	0.006	0.055	0.70564	(±2; 2σ)	0.006

The $\delta^{13}C$-$\delta^{18}O$ data of carbonates from quartz-carbonate veins from the Amalia and Kalahari Goldridge deposits are derived from Adomako-Ansah *et al.* (2017) and Hammond *et al.* (2007) respectively and also summarized in Table 2.

6. Discussion

The analytical results indicate very low Rb/Sr ratios (<1) for the vein carbonates from both deposits, suggesting that the corresponding $^{87}Sr/^{86}Sr$ ratios remained unchanged through time making the measured values a good approximation for the initial $^{87}Sr/^{86}Sr$ ratios. Consequently, the $^{87}Sr/^{86}Sr$ ratios are suitable for monitoring the nature and evolution of the ore-forming fluid(s) in the Kraaipan-Amalia terrane.

Figure 8 illustrates a binary plot of $^{87}Sr/^{86}Sr$ ratios and their corresponding Sr concentrations in vein carbonates from the Kalahari Goldridge and Amalia gold deposits, which shows that the vein carbonates from both deposits plot have a common minimum value characterized by $^{87}Sr/^{86}Sr$ isotopic ratio of 0.70354. The minimum value suggests that the ore-forming fluids for both deposits possibly originated from a common fluid reservoir source of uniform isotopic composition ($^{87}Sr/^{86}Sr$ ratio = 0.70354), which is consistent with a mantle or mafic igneous signature for the ore-forming fluids. The plot also illustrates a diverging trend towards increasing radiogenic Sr values along different evolutionary flow paths for each of the quartz-carbonate veining events in the deposits. The–increasing radiogenic Sr trend can be attributed to isotopic exchange resulting from the mixing of multiple fluids of isotopically different signatures or by the water-rock interaction between ore-forming fluids and supracrustal wall rocks with higher radiogenic Sr concentrations. The fluid inclusion and stable isotope data (Hammond *et al.* 2007; Adomako-Ansah *et al.* 2017) are inconsistent with the involvement of multiple fluids in both deposits. Hence, the effect of fluid mixing is consequently ruled out. Thus, the trend to higher $^{87}Sr/^{86}Sr$ ratios illustrated in Figure 7 can be related to isotopic exchange between ore-forming fluids and the supracrustal rocks that surround the deposits. The basement rocks to the BIF-hosted Kalahari Goldridge and Amalia gold deposits are Archean TTGs of similar age and petrographic characteristics. If the ore-forming fluids interacted with only the basement TTG rocks and/or BIF units, it is expected that the deposits will exhibit similar variations or tendencies in the radiogenic Sr isotopic ratios of their respective vein carbonates. However, this is not the case. Inconsistency in the trend to higher Sr isotopic ratios between the two deposits is illustrated in Figure 7, by comparing the Sr isotopic data with the $\delta^{13}C$ values from both deposits (e.g., Kerrich *et al.* 1987, Morishita and Nakano 2008). The vein carbonates from the Amalia gold deposit are characterized by relatively homogeneous and less radiogenic $^{87}Sr/^{86}Sr$ ratios. On the other hand, the $^{87}Sr/^{86}Sr$ ratios in the vein carbonates from the Kalahari Goldridge deposit are relatively heterogenous, more radiogenic and widespread: ranging from low values that are similar to that of the Amalia gold deposit to much higher radiogenic values that are not recorded in the Amalia gold deposit. Since the basement rocks are the same for both deposits, the analogy, therefore, would be that the wider spread to relatively higher radiogenic Sr isotopic values in the precipitating vein carbonates at the Kalahari Goldridge deposit resulted from the water-rock interaction between ore-forming fluids and the graphite-bearing metasedimentary rock surrounding

 doi:10.20944/preprints202408.2025.v1

the host BIF unit. In addition, the heterogeneous nature of the $^{87}Sr/^{86}Sr$ ratios at Kalahari Goldridge can be attributed to larger volume of fluid interaction with more crustal rocks, and relatively more intensive fluid-rock interaction. The large fluid volume is reflected by the large quartz veins (Group IIB veins) and the multiple ladder veins (Group IIA) (Hammond and Morishita 2009). Conversely, the homogeneous $^{87}Sr/^{86}Sr$ ratios in the vein carbonates from Amalia, as illustrated in Figure 7, can be attributed to interaction of ore-forming fluids with limited or restricted variety of crustal sedimentary host rocks at Amalia in comparison with Kalahari Goldridge. The observations at the Kraaipan-Amalia is consistent with several orogenic gold deposit of variable geological setting worldwide (e.g.,Goldfarb and Groves, 2015; Kerrich *et al.*,1987). For example, the review by Goldfarb and Groves (2015) on fluid and metal sources for orogenic gold deposits reported that strontium was derived from basement rocks below Archean greenstone belts that host these deposits or reflect a significant mantle component, with values altered along the flow path and at the site of gold deposition by host metasedimentary rock sequences. They also documented local wall rock sources for Sr or multiple strontium sources in host rocks distal to the gold deposits. Kerrich *et al.* (1987) noted the uniformity of initial $^{87}Sr/^{86}Sr$ ratios of mafic volcanic rocks in gold deposit-hosted terranes in the Archean Abitibi sub-province of Canada to be consistent with a homogenous upper mantle reservoir. In a similar study, the variations in $^{87}Sr/^{86}Sr$ ratios in epithermal gold deposits hosted in both the basement carbon-rich metasedimentary rocks of the Shimanto Group and the overlying andesitic volcanic rocks were investigated by Morishita and Nakano (2008) in the Kyushu region of Japan and showed relatively high $^{87}Sr/^{86}Sr$ ratios in ore-related calcite, which were inferred to indicate hydrothermal ore-forming fluid interaction with the carbon-rich metasedimentary rocks that contained much higher $^{87}Sr/^{86}Sr$ composition than the surrounding shallower volcanic rocks hosting the deposits.

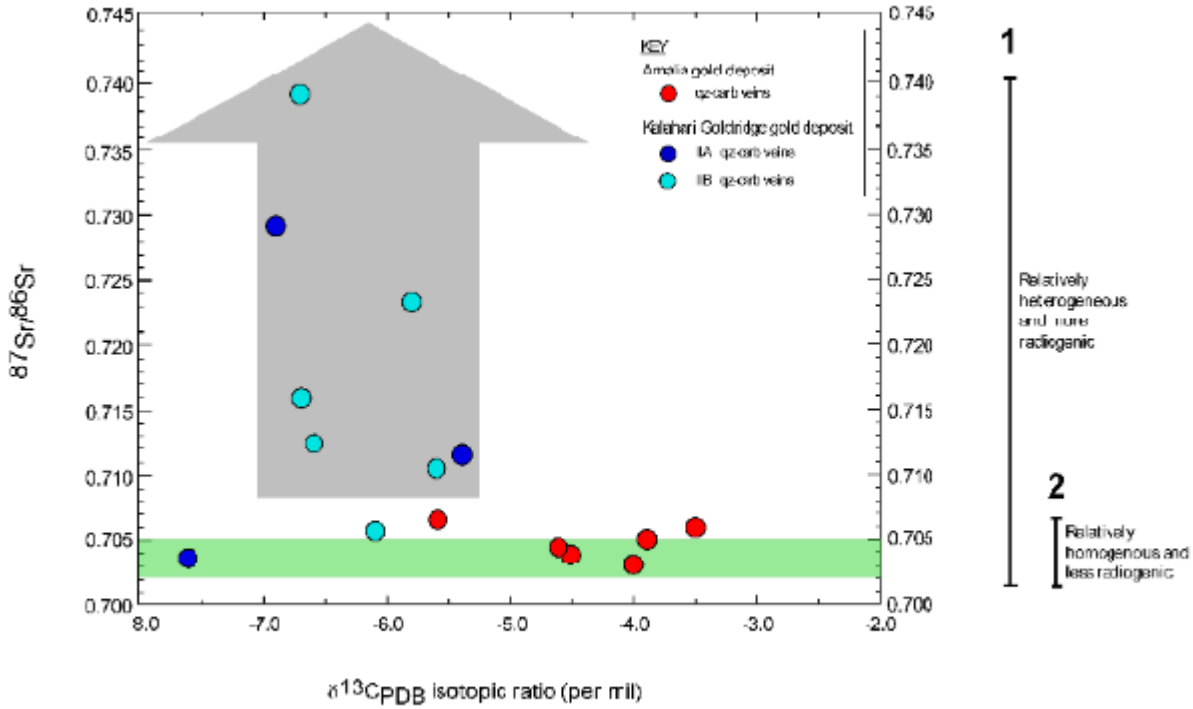

Figure 8: Plot of $^{87}Sr/^{86}S$ versus $\delta^{13}C$ of carbonates in mineralizing quartz-carbonate veins at the Kalahari Goldridge and Amalia gold deposits.

Like most Archean orogenic gold deposits, the deposits in the Kraaipan-Amalia terrane exhibit similarities in $\delta^{18}O_{water}$ values in quartz from the quartz-carbonate veins; in addition to the pervasive carbonatization and sulphidation mentioned earlier (Hammond *et al.* 2007, Adomako-Ansah *et al.* 2017). However, variations exist in the $\delta^{13}C$ values of the associated carbonates from both deposits (Figure 8). On the basis of geochemical mass balance calculations, variation in $\delta^{13}C$ values above or below average mantle/igneous values of -5±3 ‰ (Ohmoto and Rye 1979; McCuiag and Kerrich 1998; Giuliani *et al.* 2014) has been attributed to basement rocks of heterogeneous TTG

 doi:10.20944/preprints202408.2025.v1

composition (Kerrich *et al.* 1987) or water-rock interactions between ore-forming fluids and carbon-rich sedimentary rocks (e.g., Morishita and Nakano 2008, Kerrich 1987). Figure 8 shows that the $\delta^{13}C$ values of ore-related carbonates from the Kalahari Goldridge deposit (-7.6 to -5.4‰; Hammond *et al*. 2007) is lower than the $\delta^{13}C$ values of the Amalia gold deposit (-5.8 to -3.5‰; Adomako-Ansah *et al*., 2017). In addition, the CO_2-bearing ore-forming fluid at the Amalia gold deposit contains negligible CH_4 concentration whereas CH_4 is appreciable in the ore-forming fluid at Kalahari Goldridge deposit (Figure 6). While the presence of CH_4 is interpreted to be due to interaction between the ore-forming fluid and the thick sequence of graphite-bearing metasediment that have been mapped at the Kalahari Goldridge deposit (Hammond *et al.* 2007), an alternative explanation that cannot be ruled out is that the ore-forming fluid possibly evolved under reduced conditions at the time of mineralization at the Kalahari Goldridge region and that the presence of the graphite-bearing metasediment buffered the reduced conditions during gold precipitation (e.g., Morishita and Nakano 2008).

As noted earlier, carbon-rich metasediments host rocks have not been observed at the Amalia gold deposit at the time of this investigation nor has it been reported by previous workers (e.g., Kiefer 2004). This reasonably explains the absence of CH_4 in the Amalia ore-forming fluid. However, it is geologically unrealistic to ignore a probable occurrence of carbon-rich metasediment within Archean BIFs. Therefore, an alternative explanation for the lack of CH_4 contents in the fluid inclusions at Amalia could be that the probable interaction of any sort between the fluid and (thin sequence of) carbon-rich metasediment did not alter the fluid chemistry at Amalia. Therefore, in contrast to the Amalia gold deposit, the occurrence of relatively thick sequence of carbon-rich metasedimentary rocks surrounding the Kalahari Goldridge deposit could have partly buffered the ore-forming fluid to reduced conditions, thereby resulting in lower $\delta^{13}C$ values and the trend to higher $^{87}Sr/^{86}Sr$ ratios at the Kalahari Goldridge deposit. This could be one major explanation for the observed difference in redox conditions at the deposits.

The $\delta^{13}C$ and $\delta^{18}O$ of vein carbonates from the Kalahari Goldridge and Amalia gold deposits show a general positive correlation (Figure 9). However, in comparison with the Kalahari Goldridge deposit, the Amalia deposit exhibits relatively higher $\delta^{13}C$ and $\delta^{18}O$ values between the oxygen and carbon isotope ratios of carbonate samples. This observation suggest a progressive enrichment of ^{18}O and ^{13}C in the fluids during fluid interaction with host rocks from Kalahari Goldridge to Amalia. Rye and Ohmoto (1974) and Ohmoto and Rye (1979) documented such positive variation in several studied individual deposits that showed increasing trend of enrichment of ^{18}O and ^{13}C in carbonates in the paragenetic sequence of the mineralization. Ohmoto and Rye (1979) attributed this trend to (i) decreasing temperature, (ii) increasing CO_2/CH_4 ratios in an evolving fluid system resulting from local fluid interaction with graphitic rocks or immiscible separation of $CO_2 + CH_4$ in the hydrothermal fluid, and/or (iii) contribution of CO_2 from other sources resulting in a progressive increase in the $^{13}C/^{12}C$ and $^{18}O/^{16}O$ ratios. Therefore, the general positive variation between $\delta^{13}C$ and $\delta^{18}O$ in the two deposits can be attributed to increasing oxidation state in an evolving fluid system from a unique homogenous origin that is conformable with the observed $^{87}Sr/^{86}Sr$-Sr variation illustrated in Figure 8. This can be accounted for by the variation of CH_4 and CO_2 concentration, as well as decreasing mineralization temperatures from the Kalahari Goldridge to the Amalia deposit as evidenced from the chlorite geothermometry (Figure 7). The differences in the degree of ^{18}O and ^{13}C enrichments of the carbonates in Amalia and Kalahari Goldridge may however be associated with the interaction of the ore-forming fluid with different set of host rocks during mineralization in these deposits. In particular, the vein-forming fluids interacted with sedimentary rocks having organic materials at Kalahari Goldridge in comparison with the host rocks at Amalia, which lacked or have limited organic materials. The observed trend is also consistent with the decreasing temperature trend observed from Amalia to the Kalahari Goldridge deposit (Figure 7). It is worth noting that despite the different temperatures, calculations of fluid C-O isotopic compositions (i.e. $\delta^{13}C_{\Sigma C}$ and $\delta^{18}O_{H2O}$) from vein carbonate and vein quartz samples overlap mantle and mantle-derived values (Figure 8); as also indicated by the Sr isotopic compositions. This suggests that upward-migrating deep crustal ore-forming fluids having mantle-like signatures were associated with the gold mineralization in the deposits. More importantly, the slight deviations in the $\delta^{13}C_{\Sigma C}$ and $\delta^{18}O_{H2O}$ values from the mantle

 doi:10.20944/preprints202408.2025.v1

box plot in Figure 8 are consistent with the hypothesis that the fluids interacted with supracrustal rocks of high isotopic composition en route to the depositional sites in the Kraaipan-Amalia terrane; as also revealed by the Sr isotopic compositions.

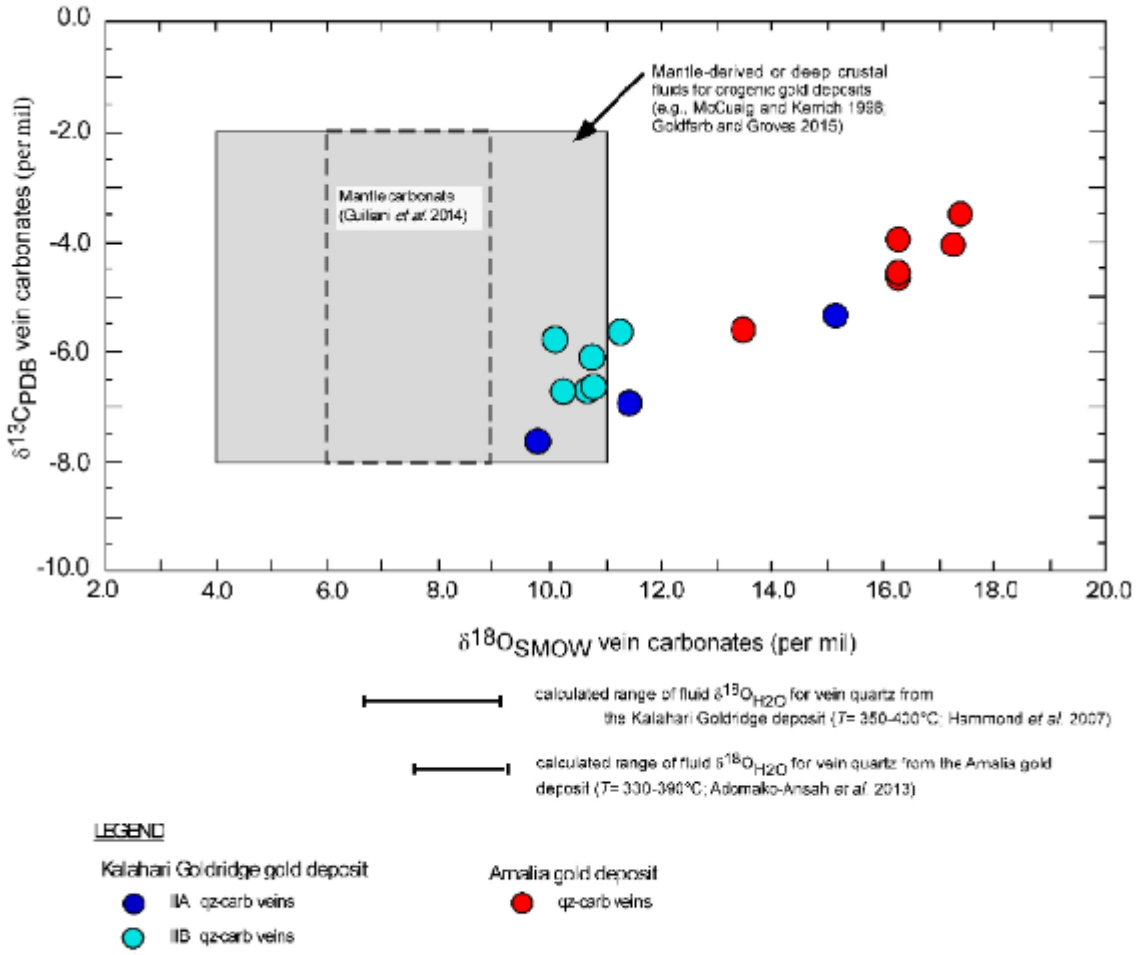

Figure 9: Variation of carbon and oxygen isotope composition in carbonates frommineralizing quartz-carbonate veins at the Kalahari Goldridge and Amalia gold deposits.

7. Conclusion

The combination of Sr, C, and O isotopic data from the Kalahari Goldridge and Amalia BIF-hosted gold deposits have been used to evaluate the nature and evolution of the ore-forming fluids associated with gold mineralization in the Kraaipan-Amalia region of South Africa. A schematic model of the Kraaipan-Amalia gold mineralization system is illustrated in Figure 10. The two gold deposits show a common source for the ore-forming fluids on the basis of Sr isotopic data acquired on carbonates associated with the gold mineralization, irrespective of their contrasting ambient redox conditions, fluid chemistry, and temperatures of gold formation.

 doi:10.20944/preprints202408.2025.v1

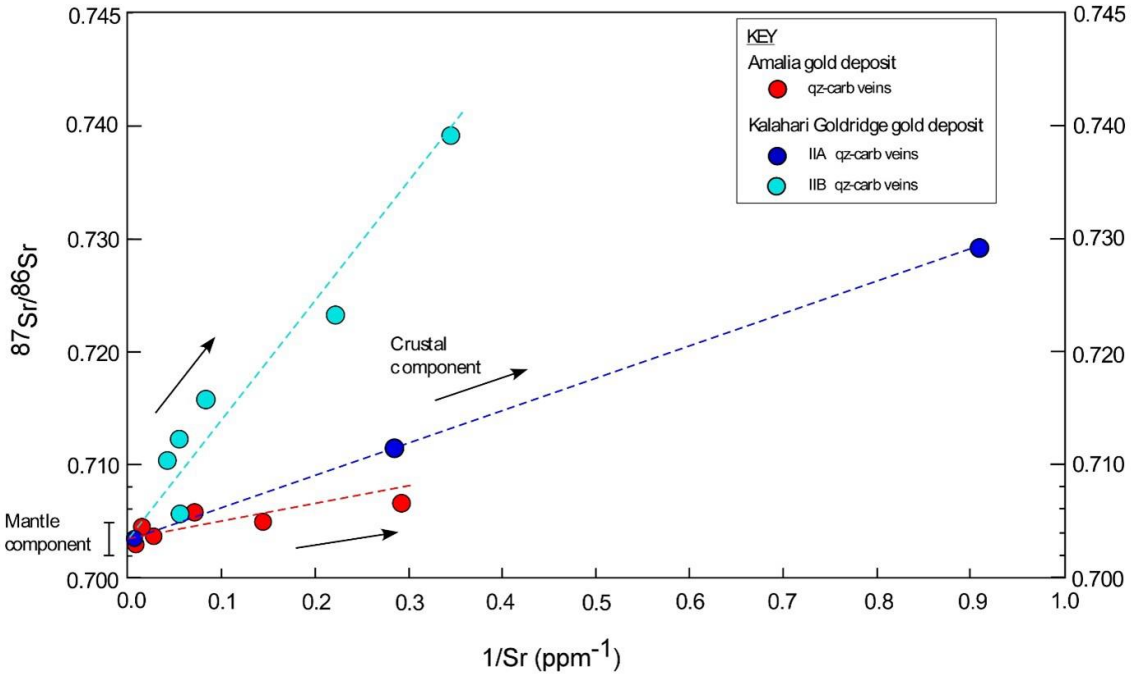

Figure 10: A plot of $^{87}S/^{86}S$ versus 1/Sr depicting the evolutionary trend of ore-forming fluids at the Kalahari Goldridge and Amalia gold deposits.

The absolute timing of the gold mineralization in these greenstone belts is not constrained, however evidence from fluid composition data and Sr-C-O isotopic ratios suggests that observed differences in redox conditions in these deposits could be attributed to different flow pathways by the evolving fluid from a common source (with minimum $^{87}Sr/^{86}Sr$=0.70354) to the sites of gold deposition. Fluid-rock interaction between ore-forming fluid and carbonaceous meta-pelitic rock units partly resulted in reducing conditions and heterogeneity in the observed Sr-C isotopic distribution at the Kalahari Goldridge deposit. On the contrary, the oxidized character and homogeneous Sr-C isotopic distribution observed at the Amalia gold deposit is attributed to the lesser fluid-rock interaction between the ore-forming fluid and limited amount of (carbonaceous) supracrustal rocks. The results of the studies amplify the fact that although Archean orogenic gold deposits formed from fluids of similar composition in similar tectonic environments, minor differences in the deposits could be linked to variable host rock composition, redox conditions of gold formation and/or other physico-chemical parameters at individual deposits.

Acknowledgments: Prof Maruyama Yamamoto, formerly of Akita University, Japan, is specially thanked for his immense support during the Sr isotope analytical runs. We also thank Prof Toshio Mizuta for his advice during the course of this research. .

References

1. Adomako-Ansah, K., Mizuta, T., Hammond, N.Q., Ishiyama, D., Ogata, T., and Chiba, H., 2013. Gold mineralization in banded iron formation in the Amalia greenstone belt, South Africa: a mineralogical and sulfur isotope study: Resource Geology, v. 63, p. 119-140.
2. Adomako-Ansah, K., Mizuta, T., Ishiyama, D., and Hammond, N.Q., 2017. Nature of ore-forming fluid and formation conditions of BIF-hosted gold mineralization in the Archean Amalia greenstone belt, South Africa: constraints from fluid inclusion and stable isotope studies: Ore Geology Reviews, v. 89, p. 609-626.
3. Anhaeusser, C., R., and Walraven, F., 1999. Episodic granitoid emplacement in the western Kaapvaal Craton: evidence from the Archean-Kraaipan granite-greenstone terrane, South Africa: Journal of African Earth Sciences, v. 28, p. 289-309.
4. Armstong, R.L., 1968. A model for the evolution of strontium and lead isotopes in a dynamic earth: Reviews of Geophysics, v. 6, 175-199.
5. Bickle, M.J., 1994. The role of metamorphic decarbonation reactions in returning strontium to the silicate sediment mass: Nature, v. 367, p. 699-704.

6. Bottinga, Y., 1968. Calculation of fractionation factors for carbon and oxygen isotopic exchange in the system calcite-carbon dioxide-water: Journal of Physical Chemistry, v. 72, p. 800-808.
7. Corner, B., Durrheim, R.J., and Nicolaysen, L.O., 1990. Relationships between the Vredefort structure and the Witwatersrand basin within the tectonic framework of the Kaapvaal Craton as interpreted from regional gravity and aeromagnetic data: Tectonophysics, v. 171, p. 49-61.
8. Deer, W.A., Howie, R.A., and Zussman, J., 1966. An Introduction to the rock forming minerals: London, Longman, 528 p.
9. de Wit, M.J., Roering, C., Hart, R.J., Armstrong, R.A., de Ronde, C.E.J., Green, R.W.E., Tredoux, M., Peberdy, E., and Hart, R.A., 1992. Formation of an Archaean continent: Nature, v. 357, p. 553-562.
10. de Wit, M. and Tinker, J., 2004, Crustal structures across the central Kaapvaal craton from deep-seismic reflection data: South African Journal of Geology, v. 107, p. 185-206.Donnelly, C.L., Griffin, W.L., O'Reilly, S.L, Pearson, N.J., Shee, S.R., 2011. The Kimberlites and related rocks of the Kuruman Kimberlite Province, Kaapvaal Craton, South Africa: Contributions to Mineralogy and Petrology, v. 161, p. 351-371
11. Eriksson, P.G., Banerjee, S., Nelson, D.R., Rigby, M.J., Catuneanu, O., Sarkar, S., Roberts, R.J., Ruban, D., Mtimkulu, M.N., and Raju, P.V.S., 2009. A Kaapvaal craton debate: Nucleus of an early small supercontinent or affected by an enhanced accretion event? Gondwana Research, v. 15, p. 354-372.
12. Goldfarb, R.J., and Groves, D.I., 2015. Orogenic gold: common or evolving fluid and metal sources through time: Lithos, v. 233, p. 2-26.
13. Groves, D.I., Goldfarb, R.J., Gebre-Mariam, M., Hagemann, S.G., and Robert, F., 1998. Orogenic gold deposits–a proposed classification in the context of their crustal distribution and relationship to other gold deposit types: Ore Geology Reviews, v. 13, p. 7-27.
14. Groves, D.I., Santosh, M., Deng, J., Wang, Q., Yang, L., and Zhang, L., 2020. A holistic model for the origin of orogenic gold deposits and its implications for exploration. Mineralium Deposita, v. 55, p. 275–292.
15. Giuliani, A., Phillips, D., Kamenetsky, V.S., Fiorentini, M.L., Farquhar, J., and Kendrick, M.A., 2014. Stable isotope (C, O, S) compositions of volatile-rich minerals in kimberlites: A review: Chemical Geology, v. 374-375, p. 61-63.
16. Hammond, N.Q., and Moore, J.M., 2006. Archean lode gold mineralization in banded iron formation at the Kalahari Goldridge deposit, Kraaipan greenstone belt, South Africa: Mineralium Deposita, v. 41, p. 483-503.
17. Hammond, N.Q., Moore, J.M., and Sheets, R.W., 2007. Physico-chemical conditions of ore-bearing fluids associated with the genesis of the Kalahari Goldridge deposit, Kraaipan greenstone belt, South Africa: Ore Geology Reviews, v. 30, p. 106-134.
18. Hammond, N.Q., and Morishita, Y., 2009. Source of ore fluids at the Kalahari Goldridge deposit, Kraaipan greenstone belt, South Africa: evidence from Sr, C and O isotope signatures in carbonates: Geofluids, v. 9, p. 356-364
19. Ho, S.E. Groves, D.I McNaughton, N.J. Mikucki, E.J. (1992). The source of ore fluids and solutes in Archaean lode-gold deposits of Western Australia, Journal of Volcanology and Geothermal Research, v. 50, p. 173-196,
20. Jacobsen, S.B., and Pimentel-Klose, M.R., 1988. Nd isotopic variations in Precambrian banded iron formations: Geophysical Research Letters, v. 15, p. 393-396.
21. Jones, I.M., and Anhaeusser, C.R., 1993. Accretionary lapilli associated with Achaean banded iron formations of the Kraaipan Group, Amalia greenstone belt, South Africa: Precambrian Research, v. 61, p. 117-136.
22. Kato, Y., Ohta, I., Tsunematsu, T., Watanabe, Y., Isozaki, Y., Maruyama, S., and Imai, N. (1998). Rare earth element variations in mid-Archean banded iron formations: implications for the chemistry of ocean and continent and plate tectonics: Geochimica Cosmochimica Acta, v. 62, p. 3475-3497.
23. Kato, Y., Yamaguchi, K.E., and Ohmoto, H., 2006, Rare earth elements in Precambrain banded iron formations: Secular changes of Ce and Eu anomalies and evolution of atmospheric oxygen, In Kessler, S.E. and Ohmoto, H, eds., Evolution of early earth's atmosphere, hydrosphere, and biosphere-constraints from ore deposits: Geological Society of America Memoir, v. 198, p. 269-289.
24. Kerrich, R., 1987. The stable isotope geochemistry of Au-Ag vein deposits in metamorphic rocks. In Kyser, T.K., ed., Stable isotope geochemistry of low temperature processes: GAC-MAC short course v. 11, p. 318-361.
25. Kerrich, R., 1989, Geochemical evidences of the sources of fluids and solutes for shear zone hosted mesothermal gold deposits. In Mineralization and Shear Zones. Edited by J.T. Bursnall. Short Course Volume 6, Geological Association of Canada
26. Kerrich, R., Fryer, B.J., King, R.W., Willmore, L.M., and van Hees, E., 1987, Crustal outgassing and LILE enrichment in major lithosphere structures, Archean Abitibi greenstone belt: evidence on the source reservoir from strontium and carbon isotope tracers: Contributions to Mineralogy and Petrology, v. 97, p. 156-168.

 doi:10.20944/preprints202408.2025.v1

27. Kiefer, R., 2004, Regional geology, tectonic evolution, and controls of gold mineralization in the Archean Amalia greenstone belt, South Africa [Ph.D. thesis]: Johannesburg, University of the Witwatersrand, 542 p.
28. McCuaig, T.C., and Kerrich, R., 1998, P-T-t-deformation-fluid characteristics of lode gold deposits: evidence from alteration systematics. Ore Geology Reviews, v. 12, p. 381-453.
29. McCourt, S., 1995. The crustal architecture of the Kaapvaal crustal block South Africa, between 3.5 and 2.0 Ga: A synopsis: Mineralium Deposita, v. 30, p. 89-97.
30. McLennan, S.M., Taylor, S.R., McCulloch, M.T., and Maynard, J.B., 1990, Geochemical and Nd-Sr isotopic composition of deep-sea turbidites: crustal evolution and plate tectonics: Geochimica Cosmochimica Acta, v. 54 (7), p. 2015-2050.
31. Mitchell, R.H., 1995, Kimberlites, orangeites, and related rocks. New York, Plenum Press.
32. Morishita, Y., and Nakano, T., 2008, Role of basement in epithermal deposits: The Kushikino and Hishikari gold deposits, southwestern Japan: Ore Geology Reviews, v. 34, p. 597-609.
33. Ohmoto, H., and Rye, R.O., 1979, Isotopes of sulphur and carbon. *in* Barnes, H.L., ed., Geochemistry of Hydrothermal Ore Deposits, 2nd Edition: New York, John Wiley and Sons, p. 509-562.
34. Palmer, M.R, and Edmond, J.M., 1989, Strontium isotope budget of the modern ocean: Earth Planetary Science Letters, v. 92, p. 11-26.
35. Peucker-Ehrenbrink, B., and Miller, M.W., 2006, Marine $^{87}Sr/^{86}Sr$ record mirrors the evolving upper continental crust: Geochimica Cosmochimica Acta, v. 70 (18), p. A487.
36. Plank, T., and Langmuir, C.H., 1998. The chemical composition for subducting sediment and its consequences for the crust and mantle: Chemical Geology, v. 145, p. 325-394.
37. Poujol, M., Anhaeusser, C.R., and Armstrong, R.A., 2002, Episodic granitoid emplacement in the Archean Amalia-Kraaipan terrane, South Africa: confirmation from zircon U-Pb geochronology: Journal of African Earth Sciences, v. 35, p. 147-161.
38. Richardson, S.H., Shirey, S.B., Harris, J.W., and Carlson, R.W., 2001, Archean subduction recorded by Re-Os isotopes in eclogitic sulfide inclusions in Kimberley diamonds: Earth and Planetary Science Letters, v. 191, p. 257-266.
39. Ridley, J., and Hagemann, S.G., 1999, Interpretation of post-entrapment fluid-inclusion re-equilibration at the Three Mile Hill, Marvel Loch and Griffins Find high temperature lode-gold deposits, Yilgarn Craton, Western Australia: Chemical Geology, v. 154, p. 257–278.
40. Robb, L.J., and Meyer, F.M., 1995, The Witwatersrand Basin: Geological framework and mineralization processes: Ore Geology Reviews, v. 10, p. 67-94.
41. Rye, R.O., and Ohmoto, H., 1974, Sulphur and carbon isotopes and ore genesis: a review. Economic Geology 69, 642-826.
42. Sato, H., Ishiyama, D., Mizuta, T., and Ishikawa, Y., 1999, Rare earth element analysis of rock and thermal water samples by inductively coupled plasma mass spectrometry: Science and Technology Report, Faculty of Engineering and Resource Science, Akita Univiversity, 20, p. 1-8 (in Japanese with English abstract).
43. Schmitz, M.D., Bowring, S.A., de Wit, M.J., and Gartz, V., 2004, Subduction and terrane collision stabilize the western Kaapvaal craton tectosphere 2.9 billion years ago: Earth and Planetary Science Letters, 222, p. 363-376.
44. Shields, G.A., 2007, A normalized seawater strontium isotope curve: possible implications for Neoproterozoic-Cambrian weathering rates and the further oxygenation of the earth: eEarth, v.2, p. 35-42.
45. Shields, G.A., and Veizer, J., 2002, Precambrian marine carbonate isotope database: version 1.1.: Geochemistry, Geophysics, Geosystems, v.6, p. 1-12.
46. Smith, C.B., 1983, Pb, Sr and Nd isotopic evidence for sources of southern African Cretaceous kimberlites. Nature, v. 304, 51-54.
47. Veizer, J., 1989, Strontium isotopes in seawater through time, Annual Review Earth Planetary Science, 17, p. 141-167.
48. Yamaguchi, K.E., Bau, M. and Ohmoto, H., 2000, Constraints from REEs on the processes and environments for Precambrian banded iron formations: revaluation of the data and models. J. Goldschmidt Conference Abstract, 5 (2), p. 1110.
49. Yamamoto, M., and Maruyama, T., 1996, The Sr and Nd isotopic analysis and quantitative analysis of Rb and Sr by using MAT 261: Report of the Research Institute of Natural Resources, Mining College, Akita University, v. 61, p. 7-30 (in Japanese with English abstract).